

X-ray diffraction evidence for a monoclinic form of stibnite, Sb_2S_3 , below 290 K

SATORU KUZE,¹ DOUGLAS DU BOULAY,² NOBUO ISHIZAWA,^{2,*} ATSUSHI SAIKI,³ AND ALLAN PRING⁴

¹Interdisciplinary Graduate School of Science and Engineering, Tokyo Institute of Technology, 4259 Nagatsuta, Midori-ku, Yokohama 226-8502, Japan

²Ceramics Research Laboratory, Nagoya Institute of Technology, Gokisocho, Showa-ku, Nagoya 466-8653, Japan

³Center for Advanced Materials Analysis, Tokyo Institute of Technology, 2-12-1 Ookayama, Meguro-ku, Tokyo 152-8550, Japan

⁴Department of Mineralogy, South Australian Museum, North Terrace, Adelaide, South Australia 5000, Australia

ABSTRACT

The nature of the symmetry changes associated with phase transitions in stibnite, Sb_2S_3 , has been investigated by powder and single crystal X-ray diffraction. Above 420 K stibnite (I) is centrosymmetric $Pbnm$. Stibnite (II) is stable between 290 and 420 K and is acentric $P2_1nm$. Below 290 K stibnite (III) is stable and systematic absences indicates that this phase is monoclinic with space group $P2_1$ or Pm , or triclinic $P1$, but the cell dimensions remain geometrically orthorhombic. These findings are in agreement with variations in physical and electrical properties reported in the literature.

INTRODUCTION

Stibnite, Sb_2S_3 is the most common and widespread of antimony minerals. It occurs in hydrothermal vein systems, formed over a wide range of temperatures, but has a maximum thermal stability of 829 K (Anthony et al. 1990; Vaughan and Craig 1978).

Recently Sb_2S_3 is also attracting considerable interest as a candidate material for optoelectronic devices exploiting the different properties of amorphous and polycrystalline samples at various temperature (Arun and Vedeshwar 1996; El Zawawi et al. 1998; Rajpure and Bhosale 2000; Farid and Bekheet 2000). Arun and Vedeshwar (1996) reported on the irreversible transformation from the amorphous to the crystalline state at around 435 K that makes Sb_2S_3 suitable for use in WORM (Write Once Read Many) optical storage applications. Rajpure and Bhosale (2000) also exploited semiconducting Sb_2S_3 as a photoelectrode generating electrons and holes in a structurally reversible, rechargeable photoelectrochemical storage cell. To fully understand the mechanisms involved in these applications, accurate structural information is very important.

The room-temperature structure of stibnite is often described as having an orthorhombic unit cell with space group $Pbnm$ ($a = 11.23$, $b = 11.31$, $c = 3.84$ Å) (Hofmann 1933; Scavnicar 1960; Bayliss and Nowacki 1972; McKee and McMullan 1975). Recently, Kyono et al. (2002) adopted the same symmetry model in a low-temperature study of this material. However, dielectric permittivity measurements by Grigas and Karpus (1968) indicated a first-order phase transition at 290.7 K accompanied by a decrease in spontaneous polarization from 5×10^{-2} to 1.0×10^{-2} C/m². Thereafter a further first-order phase transition was identified by Orliukas and Grigas (1974), associated with a total loss of spontaneous polarization in Sb_2S_3 above 420 K. This implies the presence of a center of symmetry in the high-temperature phase that is consistent with $Pbnm$ symmetry. Corresponding transition temperatures were also detected with ultrasonic and

pyroelectric techniques (Samulionis et al. 1974; Rinkevichius and Mikalkevichius 1967), revealing the absence of symmetry centers in these crystals at ambient and low temperatures, though over a somewhat broader range of transition temperatures of 270–340 and 420–490 K. Lukaszewicz et al. (1997) confirmed that at 320 K stibnite (II) has $P2_1nm$ symmetry while the high-temperature form was predicted to be $Pbnm$ in accord with the reported physical properties. The structure and symmetry of the low-temperature form, stibnite (III) remain unresolved.

The crystal structure of stibnite (I) (Fig. 1) consists of infinite $[\text{Sb}_2\text{S}_3]$ ribbons parallel to c . Four ribbons pass through the cell, combined together pairwise forming $[\text{Sb}_4\text{S}_6]$ chains. In a $[\text{Sb}_4\text{S}_6]$ ribbon, the Sb and S atoms are linked together by short covalent bonds (2.52 to 2.54 Å) (McKee and McMullan 1975). The Sb and S atoms of neighboring $[\text{Sb}_4\text{S}_6]$ ribbons are weakly linked; Sb-S contacts are in the range 3.11 to 3.64 Å, with the Sb lone-pair spreading into the inter-ribbon space perpendicular to c (Kyono et al. 2002).

In stibnite (I), $Pbnm$ above 420 K, the four Sb_2S_3 units are symmetry equivalent. Below this temperature the space group becomes $P2_1nm$, [stibnite (II)], and there are two kinds of Sb_2S_3 units in a $[\text{Sb}_4\text{S}_6]$ ribbon due to the breaking of the centre of symmetry. The loss of the centre is associated with displacements of the outer S atoms of the $[\text{Sb}_4\text{S}_6]$ ribbon in the a - b plane perpendicular to c . The far-infrared studies of Petzelt and Grigas (1973) suggest that further symmetry breaking may not occur during the phase transition from stibnite (II) to stibnite (III) at or near room temperature. We present here the results of a study into the changes of symmetry associated with the structure transformations in stibnite between 200 and 350 K.

MATERIALS AND METHODS

Stibnite crystals from Bauiti, Romania were used in this study (South Australian Museum G23390). The composition of the sample was checked by microprobe analyses, performed with a EDAX EAGLE μ -Probe, and a wavelength-dispersive spectrometer on a Phillips PW2404 instrument. The analysis revealed that the sample was pure Sb_2S_3 and no other elements were detected in concentrations above trace levels. The temperature dependency of the cell parameters was investigated using a Philips PW3050 powder X-ray diffractometer with $\text{CuK}\alpha$ radiation, oper-

* E-mail: ishizawa@nitech.ac.jp

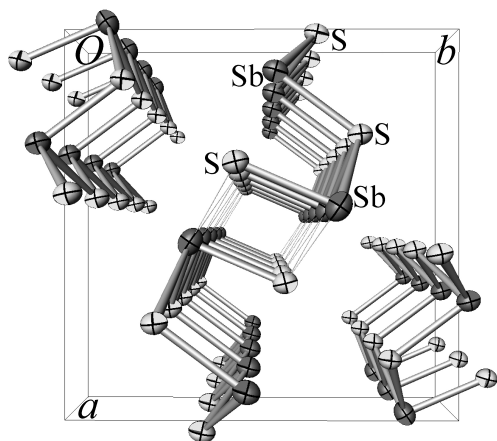


FIGURE 1. A perspective view of the crystal structure of Sb_2S_3 , c -axis projection.

ated at 40 kV and 30 mA, with a scan speed of $0.6^\circ/\text{min}$ in 2θ , a 1° divergence slit, and a 0.2 mm receiving slit. The data was obtained from 10° to 60° in 2θ with a step width of 0.02° . The sample temperature was controlled to within ± 0.1 K with a Phillips TTK450 module attached to the diffractometer.

Crystals were crushed and ground into a fine powder and mixed with Si powder for internal calibration. Powder patterns were measured at a range of temperatures from 100 to 470 K and in particular, at 10 K intervals between 200 and 350 K. The heating speed was 10 K min^{-1} . The samples were held at temperature for 10 minutes to ensure thermal equilibrium before each diffraction pattern was collected. Using the known thermal expansion coefficient of silicon (Batchelder and Simmons 1964) and the standard Si lattice parameters from JCPDS, zero-offset errors were identified and corrected. All refinements were undertaken with the FULLPROF-2000 program package (Rodríguez-Carvajal 1993). After determining zero offset and background parameters using the Si component at each temperature, the unit cell and profile parameters of Sb_2S_3 were refined. Atomic coordinates were fixed at those determined by Kyono et al. (2002).

Additional single crystal X-ray diffraction experiments were undertaken to determine space group extinction rules to help identify the low temperature symmetry. A horizontal-type four-circle diffractometer mounted on beam line 14A of the Photon Factory, High Energy Accelerator Research Organization was used (Satow and Iitaka 1989). Vertically polarized X-rays of 0.75035 \AA wavelength were diffracted from the sample and this was calibrated by initial checks using a spherically ground standard Si crystal. Scattered X-rays were detected with an eight-channel avalanche photodiode point detector with around 75% detection efficiency (Kishimoto et al. 1998). Custom designed Diff14A software was used to drive the goniometer. The sample temperature was controlled by an Oxford Cryosystem, dry nitrogen gas-blowing cooler.

The sample size was approximately $80 \times 50 \times 50 \mu\text{m}^3$. The diffracted intensity of the strongest reflection (020) marked approximately 120 000 cps. Because the weak reflections in concern in the following section had intensities less than 1000 cps at most, the use of synchrotron X-rays was essential for the study of systematic extinction rules.

RESULTS AND DISCUSSION

From the powder diffraction studies, the unit cell dimensions were determined over the temperature range 100 to 470 K (Fig. 2). Those at 280, 300, and 430 K are listed in Table 1. For each of a , b , and c there is a monotonic increase in dimension with temperature. The most important feature for our purposes, however, is the subtle but discernable change in the rate of increase with temperature which occurs at around 290 K for both the a and b cell parameters in Figures 2a–b. Similar changes, though not so readily discernable, occur with the c parameter (Fig. 2c). A change in the rate of thermal expansion is evidence of a phase transition of some description, either electronic or structural. The temperature at which the rate of expansion changes is in agreement with the 290.7 K phase transition reported by Grigas and Karpus (1968).

The observed difference in temperature dependence of cell parameters is quite plausible given the nature of the crystal structure, infinite $[\text{Sb}_4\text{S}_6]$ ribbons running parallel to c . The short and strong covalent bonding within the $[\text{Sb}_2\text{S}_3]$ ribbons propagating along the c -axis should behave quite rigidly, dominating any lattice expansion modes along this axis. On the other hand, considerably longer and weaker intra-ribbon bonding occurs in the a - b plane, normal to the c -axis. This bonding involves greater distances with shallower potentials and includes repulsive terms between lone-pair electrons of Sb 5s and the S^{2-} anion. The interplay between these weaker attractive and repulsive forces is far more susceptible to temperature-dependent variations, and is thus quite consistent with the observed changes in the rate of expansion of the a and b lattice parameter variations shown in Figure 2.

If the observed changes do reflect a phase transition, it could well be not only purely electronic but also structural. Most materials exhibiting phase transitions tend to adopt lower symmetry lattices at lower temperatures as formerly equivalent atomic sites become inequivalent. If the transitions involve breaking of glide plane or improper rotation symmetries, then these can often be detected as violations of the systematic extinction rules of the

TABLE 1. Lattice parameters of stibnite

	280 K	300 K	430 K
a (Å)	11.2335(9)	11.2370(9)	11.2608(10)
b (Å)	11.3144(9)	11.3170(9)	11.3397(10)
c (Å)	3.8342(2)	3.8353(2)	3.8438(3)

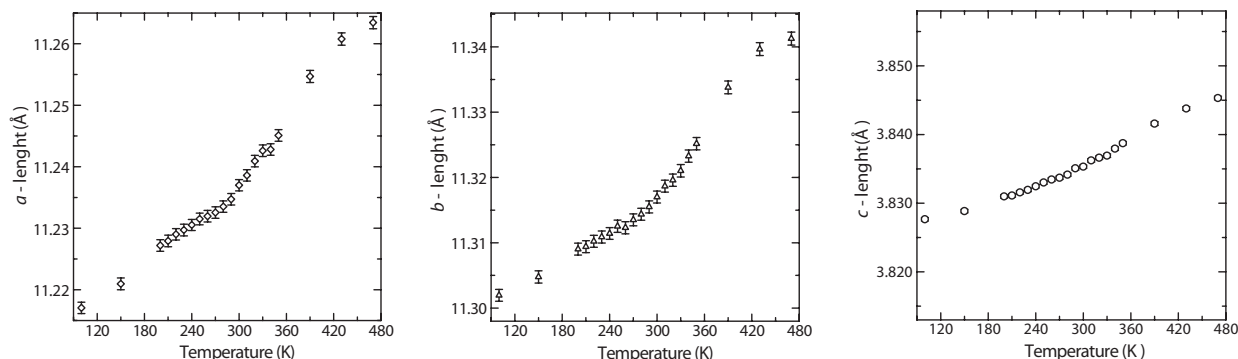


FIGURE 2. Temperature dependencies of cell parameters a (a), b (b), and c (c).

higher symmetry. In stibnite the reported stibnite (I) structure adopts $Pbnm$ symmetry, involving 2_1 screw axes along each of **a**, **b**, and **c**, with an improper mirror normal to the **a**-axis corresponding to a *b*-glide, and an improper mirror normal to the **b**-axis corresponding to the *n*-glide. In the reported low symmetry stibnite (II) structure, the *b*-glide is broken leaving $P2_1nm$ symmetry (Lukaszewicz et al. 1997)

The *b*-glide diffraction extinction rules imply that reflections in the $0kl$ series with *k* odd should be systematically extinguished. To see if this is true for stibnite we used single crystal X-ray diffraction to measure the 014 reflection at several temperatures, results of which are shown in Figure 3a. Reflection profiles as the crystal was rotated into the diffracting condition were examined using a $2\theta/\omega$ scan method within the range of 1.5° in ω . To compare data measured at different temperatures and different times, the diffracted intensity of the reflection was calibrated against the intensity of the incident X-ray flux. The results show a well defined reflection profile at all three temperatures, though unfortunately due to technical problems low-angle data for 295 and 280 K were not measured (Fig. 3a). Other reflections from the same series, such as 052 (Fig. 3b), exhibit similar tendencies. Some also show a slightly different temperature dependence, such as the 011 reflection shown in Figure 3c. Although these reflections are relatively weak, and might be attributed to multiple scattering from simultaneous excitation of other strong reflections coincident with the Ewald sphere, we believe that they imply broken *b*-glide symmetry of the $Pbnm$ lattice, reducing it to $P2_1nm$ as proposed by Lukaszewicz et al. (1997).

In addition to the *b*-glide violations, the $h0l$ series, with $h+l$ odd, were also examined for violations of the *n*-glide with an improper mirror normal to **b**. Figure 4a shows the $40\bar{1}$ reflection as evidence of this symmetry violation. Figure 4b shows the 500 reflection, which also satisfies the *h*-odd condition for the $h00$ series, violating the 2_1 screw element parallel to **a** that becomes manifest at low temperature.

If the transition from stibnite (II) to stibnite (III) is assumed to be continuous, i.e., of second order, then the only feasible symmetries are subgroups of $P2_1nm$, of which only $P11m$ and its triclinic $P1$ subgroup remain. Both groups support the low temperature experimental observations of dielectric permittivity and pyroelectricity.

On the other hand, Grigas and Karpus (1968) reported evidence of a discontinuous, i.e., first order, phase transition from stibnite (II) to stibnite (III). In that case the possible stibnite (III) symmetries should not be restricted simply to the subgroups of $P2_1nm$, but of necessity must be accessible without any gross structural transformations that would certainly be detectable in other manners. The most likely candidates involve symmetry

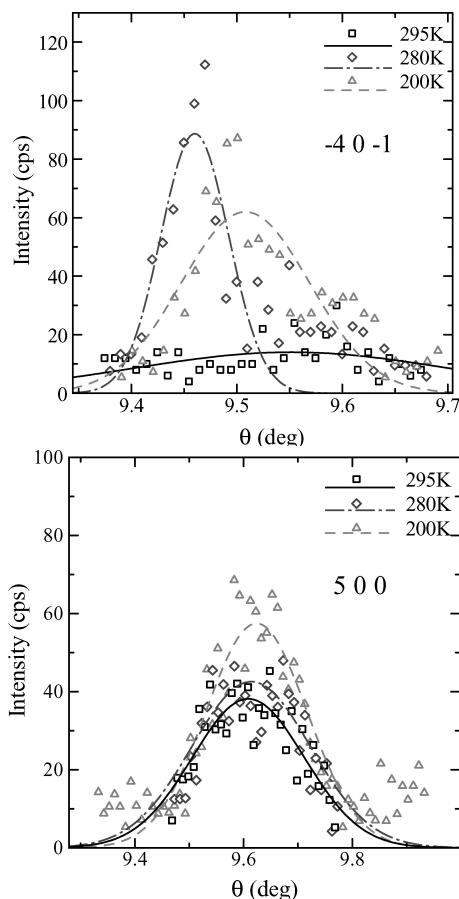


FIGURE 4. Plots of variation of peak profile with temperature for reflections of the classes $h0l$ and $h00$, (a) $40\bar{1}$ and (b) 500, respectively.

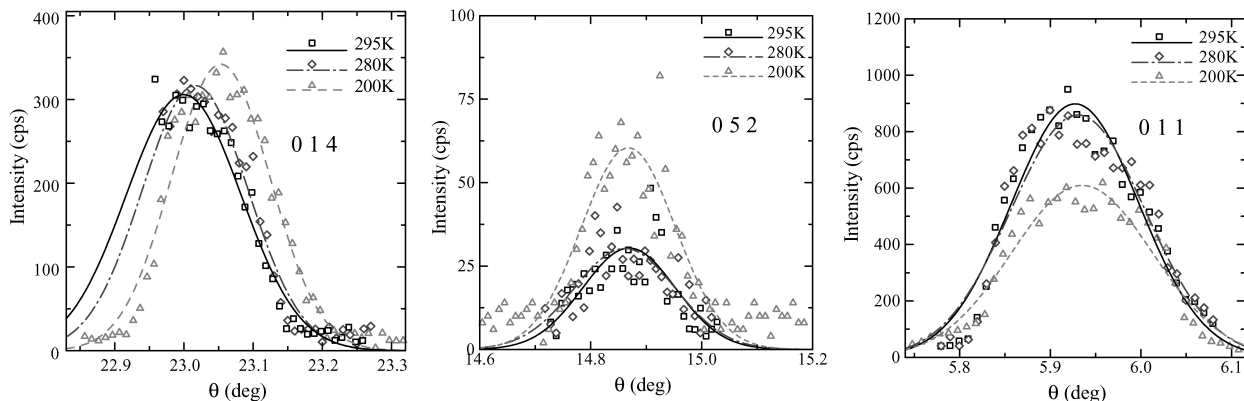


FIGURE 3. Plots of variation of peak profile with temperature for the following $0kl$ reflections: (a) 014, (b) 052, (c) 011.

elements belonging to other subgroups of the $Pbnm$, stibnite (I) parent symmetry. Having shown earlier that the b -glide along a was demonstrably broken, the only elements remaining are the 2_1 screw axes along both b and c . In our single crystal measurements no evidence of any l odd, $00l$ reflections were observed below 290 K, so that certainly a 2_1 screw along c cannot be excluded. For the k odd, $0k0$ reflection series only the 050 reflection was present at 295 K, it became weaker at 280 K and vanished by 200K as shown in Figure 5. Consequently a 2_1 screw axis along b is also quite plausible for stibnite (III).

The observations outlined above suggest that the structure of stibnite (III), occurring below 290 K, should contain elements of one or more of the monoclinic space groups; $P12_11$, $P112_1$, $P11m$, or triclinic $P1$. The only viable combination is centrosymmetric $P112_1/m$, which conflicts with the spontaneous polarization observations of Grigas et al. (1976). No other combinations of the monoclinic elements above are possible without gross structural changes to accommodate the ensuing higher orthorhombic symmetries, such as $P22_12_1$. We therefore conclude that most stibnite, at ambient temperatures, is in the monoclinic or triclinic stibnite (III) form, belonging to one of the four space groups deduced above and satisfying both the k even condition in the $0k0$ series and l even condition of the $00l$ series, to a very good approximation.

ACKNOWLEDGMENTS

This study was supported by grant-in-aid for scientific research no. 14550663, from the Ministry of Education, Culture, Sports, Science, and Technology, Japan. The financial support of the Australian Research Council is also gratefully acknowledged. The synchrotron X-ray experiments were carried out at the Photon Factory KEK under program 2002G042.

REFERENCES CITED

- Anthony, J.W., Bideaux, R.A., Bladh, K., and Nichols, M.C. (1990) Handbook of Mineralogy: Elements, Sulfides and Sulfosalts, 1, 588 pp. Mineral Data Publishing, Tucson.
- Arun, P. and Vedeshwar, A.G. (1996) Phase modification by instantaneous heat treatment of Sb_2S_3 films and their potential for photothermal optical recording. *Journal of Applied Physics*, 79, 4029–4036.
- Batchelder, D.N. and Simmons, R.O. (1964) Lattice constants and thermal expansivities of Silicon and of Calcium Fluoride between 6 and 322 K*. *Journal of Chemical Physics*, 41, 2324–2329.
- Bayliss, P. and Nowacki, W. (1972) Refinement of the crystal structure of stibnite, Sb_2S_3 . *Zeitschrift für Kristallographie*, 135, 308–315.
- El Zawawi, I.K., Abdel-Moez, A., Terra, F.S., and Mounir, M. (1998) Substrate temperature effect on the optical and electrical properties of antimony trisulfide thin films. *Thin Solid Films*, 324, 300–304.
- Farid, A.M. and Bekheet A.E. (2000) AC conductivity and dielectric properties of Sb_2S_3 films. *Vacuum*, 59, 932–939.
- Grigas, A.P. and Karpus, A. (1968) Phase transformation in the high resistance semiconductor of Sb_2S_3 . *Soviet Physic –Crystallography*, 12, 627–628.
- Grigas, J., Zadorozhnaya, L.A., Liachovitskaya, V.A., and Orliukas, A. (1976) Domain structure of Sb_2S_3 single crystals. *Lietuvos Fiz. Rinkiny*, 16,

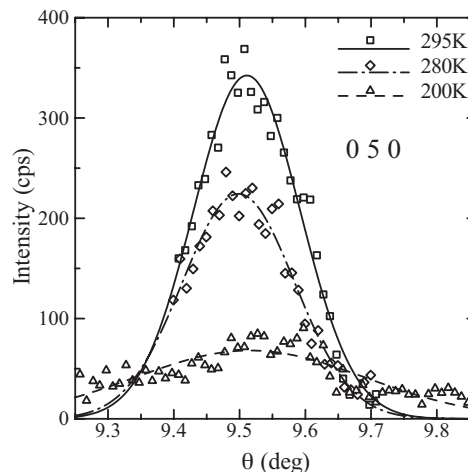


FIGURE 5. Plots of variation of peak profile with temperature for the 050 reflection.

833–839.

- Hofmann, W. (1933) Die Struktur der Minerale der Antimonitgruppe. *Zeitschrift für Kristallographie*, 86, 225–245.
- Kishimoto, S., Ishizawa, N., and Vaalsta, T.P. (1998) A fast detector using stacked avalanche photodiodes for x-ray diffraction experiments with synchrotron radiation. *Review of Scientific Instruments*, 69, 384–391.
- Kyono, A., Kimata, M., Matsuhisa, M., Miyashita, Y., and Okamoto, K. (2002) Low-temperature crystal structures of stibnite implying orbital overlap of $Sb 5s^2$ inert pair electrons. *Physics and Chemistry of Minerals*, 29, 254–260.
- Lukaszewicz, K., Pietraszko, A., Stepien-Damm, J., Grigas, J., and Kajokas, A. (1997) Crystal structure of stibnite in phase II at 320 K. *Polish Journal of Chemistry*, 71, 390–395.
- McKee, D.O. and McMullan, J.T. (1975) Comment on the structure of antimony trisulfide. *Zeitschrift für Kristallographie*, 142, 447–449.
- Orliukas, A. and Grigas, J. (1974) Phase transition in stibnite. (in Russian) *Kristallografia*, 19, 880–882.
- Petzelt, J. and Grigas, J. (1973) Far infrared dielectric dispersion in Sb_2S_3 , Bi_2S_3 and Sb_2Se_3 single crystals. *Ferroelectrics*, 5, 59–68.
- Rajpuro, K.Y. and Bhosale, C.H. (2000) Sb_2S_3 semiconductor-septum rechargeable storage cell. *Materials Chemistry and Physics*, 64, 70–74.
- Rinkevichius, V.S. and Mikalkevichius, M.P. (1967) Pyroelectric effect in antimony trisulfide single crystals. *Fizika Tverdogo Tela*, 9, 2997–2998.
- Rodriguez-Carvajal, J. (1993) Recent advances in magnetic structure determination by neutron powder diffraction. *Physica B*, 192, 55–59.
- Samulionis, V., Orliukas, A., and Grigas, J. (1974) Anomalous ultrasonic damping in Sb_2S_3 . *Fizika Tverdogo Tela*, 16, 206–208.
- Satow, Y. and Iitaka, Y. (1989) Horizontal-type four-circle diffractometer station of the vertical wiggler beamline at the Photon Factory. *Review of Scientific Instruments*, 60, 2390–2393.
- Ščavnicar, S. (1960) The crystal structure of stibnite a redetermination of atomic positions. *Zeitschrift für Kristallographie*, 114, 85–97.
- Vaughan, D.J. and Craig, J.R. (1978) *Mineral Chemistry of Metal Sulfides*. Cambridge University Press, Cambridge.

MANUSCRIPT RECEIVED SEPTEMBER 22, 2003

MANUSCRIPT ACCEPTED DECEMBER 22, 2003

MANUSCRIPT HANDLED BY KEVIN ROSSO